[AMERICAN JOURNAL OF SCIENCE, VOL. 300, JUNE, 2000, P. 463–482]

# American Journal of Science

*JUNE 2000*

## MASSIF-WIDE METAMORPHISM AND FLUID EVOLUTION AT NANGA PARBAT, NORTHERN PAKISTAN

MICHAEL A. POAGE,* C. PAGE CHAMBERLAIN,* and DAVE CRAW**

**ABSTRACT. The Nanga Parbat-Haramosh Massif (NPHM) is located in northwestern Pakistan at one of the two great syntaxial bends of the Himalayas. The NPHM has experienced a complex tectonic and metamorphic history involving at least an earlier Himalayan metamorphic event associated with subduction and crustal thickening and a later metamorphic overprint associated with rapid uplift and exhumation. Here we present the results of a massif-wide petrologic and fluid study, compiling and characterizing variations in metamorphic mineral assemblages, thermobarometric data, P-T path interpretations, and subsurface fluid compositions.**

**Metamorphic mineral assemblages reveal steep metamorphic gradients away from the granulite grade cordierite-sillimanite-bearing massif core into amphibolite facies rocks toward the flanks. New and compiled thermobarometric data show distinct variations within the massif with rocks in the rapidly denuding core recording low-pressure metamorphic conditions and rocks toward the eastern margin recording higher-pressure conditions similar to adjoining Ladakh terrane rocks. Compiled P-T paths are variable within the massif but generally show near isothermal decompression in the massif core and fragments of clockwise P-T histories toward the massif margins. We suggest that the systematic variation of mineral assemblages, thermobarometric data, and P-T paths is consistent with a recently proposed "pop-up structure" model for the NPHM, whereby recent asymmetrical structural uplift of the massif core is accommodated along high angle faults and shear zones within the massif.**

**Consistent with the pop-up structure model, fluid inclusion data from quartz veins on a transect across the massif suggest a dual hydrothermal system composed of both meteoric and metamorphic fluids. Subsurface fluids are dominantly water-rich in the massif core, becoming more $CO_2$-rich toward the eastern massif margin, suggesting that infiltration of meteoric water into the subsurface is greatest in the massif core and is driven by steep topography generated by rapid uplift. Oxygen isotope ratios of quartz veins indicate that fluids readily equilibrate with host rocks suggesting a rock-dominated hydrothermal system.**

### INTRODUCTION

The Nanga Parbat-Haramosh Massif (NPHM) is located in the northwest Himalaya of Pakistan and is a window of Indian crust surrounded on three sides by the island arc rocks of the Ladakh and Kohistan terranes. Located at one of the two corners of the Himalayas, the NPHM has experienced a complex tectonic and metamorphic history likely involving a pre-Himalayan or Precambrian metamorphic event (Treloar, Wheeler, and Potts, 1994; Wheeler, Treloar, and Potts, 1995), a Himalayan metamorphic event associated with subduction and crustal thickening (Chamberlain, Jan, and Zeitler, 1989; Treloar, Rex, and Williams, 1991; Smith, Chamberlain, and Zeitler, 1994), and a later metamorphic overprint associated with rapid surface and structural uplift and exhumation (Zeitler, 1985; Zeitler and Chamberlain, 1991; Zeitler, Chamberlain, and Smith, 1993; Winslow, Chamberlain, and Zeitler, 1995). Research activity over the past several decades has documented several anomalous characteristics of the NPHM including very

* Department of Earth Sciences, Dartmouth College, Hanover, New Hampshire 03755
** Geology Department, University of Otago, P.O. Box 56, Dunedin, New Zealand

young radiometric cooling ages, rapid uplift/exhumation, young anatexis, and active hydrothermal systems indicative of elevated geotherms beneath the massif (Zeitler, Chamberlain, and Smith, 1993; Whittington, 1996; Chamberlain and others, 1995; Winslow and others, 1994). In addition, recent work has focused on the thermomechanical development of the massif, possibly linking recent tectonism to rapid incision by the Indus River (Zeitler and Koons, 1998; Zeitler and others, ms).

Understanding the nature of the massif's metamorphic history is of utmost importance in understanding mountain development at collisional corners and in placing constraints on models characterizing the nature of crustal deformation in this unique tectonic environment. Numerous papers have discussed aspects of NPHM petrology within various tectonophysical contexts (Chamberlain, Jan, and Zeitler, 1989; Chamberlain, Zeitler, and Erickson, 1991; Pognante, Benna, and, Le Fort, 1993; Wheeler, Treloar, and Potts, 1995; Winslow, Chamberlain, and Zeitler, 1995; George and Bartlett, 1996; Le Fort, Guillot, and Pêcher, 1997; Whittington, Harris, and Baker, 1998; Whittington, Harris, and Butler, 1999). Most previous studies have focused on specific regions within massif, and to date there has been little compilation of information on the massif-scale. In addition to the complicated metamorphic history there is evidence that fluid infiltration may have played an important role during metamorphism (Chamberlain and others, 1995) and associated fluid-present anatexis (Butler, Harris, and Whittington, 1997; Whittington, Harris, and Butler, 1999). Hence, equally important in understanding the geologic history of the massif is understanding the widespread syntectonic hydrothermal activity within the massif (Craw and others, 1994, 1997; Chamberlain and others, 1995).

Thus, our objective in this study was to conduct a broad petrologic, thermobarometric, fluid inclusion, and isotopic study to characterize the metamorphic and subsurface fluid architecture of the NPHM on the massif-scale, synthesizing new information with data from previous studies. Specifically we sought to (1) construct a metamorphic mineral assemblage distribution map for the entire massif broadly outlining major assemblage boundaries, (2) construct a thermobarometric map based on previously published and new data to outline regions of different final equilibration pressures and temperatures within the massif, (3) assemble published P-T paths from NPHM rocks, (4) determine the subsurface distribution of fluid types and compositions through which metamorphosing rocks must pass en route to the surface, and (5) interpret our synthesized data in light of recent geochronologic and structural data from the NPHM.

We present new petrographic and thermobarometric data from the metamorphic rocks throughout the massif and stable isotope and fluid inclusion data from quartz veins in a transect across the massif. We find that there is a broadly concentric metamorphic pattern centered on the Nanga Parbat summit region, such that the highest-grade and lowest-pressure rocks are coincident with the highest topography and youngest radiometric cooling ages ($<$10 Ma). The massif is bordered on the east by higher-pressure metamorphic rocks, likely of Himalayan age ($\sim$30 Ma) or older. Shear zones and faults internal to the massif separate these different styles and ages of metamorphism. In addition, low-pressure rocks in the core of the massif are associated with meteoric fluids, whereas higher-pressure rocks along the border of the massif are associated with $CO_2$-bearing metamorphic fluids. These data support and place important constraints on recent tectonic models (Schneider and others, 1999) proposed for the massif and surrounding terranes.

Given that the focus of this paper is primarily on the larger-scale petrologic features of the massif, we feel that it is constructive to assemble as much of the presently available data to aid in interpretation of the massif's metamorphic and fluid history. The broad scope of this paper, however, does not allow us here to present much of the detailed analytical information about either specific original data points or data compiled from the literature.

GEOLOGIC SETTING

The Nanga Parbat-Haramosh Massif is located at the western syntaxis of the Himalaya. The massif proper (fig. 1) is a structural window of Indian crust rocks exposed through the surrounding Kohistan and Ladakh Terrane island-arc rocks of the former subduction zone (Tahirkheli and others, 1979) that were thrust over Indian plate rocks along the Main Mantle Thrust (MMT) during the Eocene (Treloar and others, 1989; Butler and others, 1992). Evidence of recent anatexis (Zeitler and Chamberlain, 1991; Whittington, Harris, and Butler, 1999) and coeval rapid uplift and exhumation (Zeitler, Chamberlain, and Smith, 1993), elevated geotherms and brittle-ductile transition (Wins-

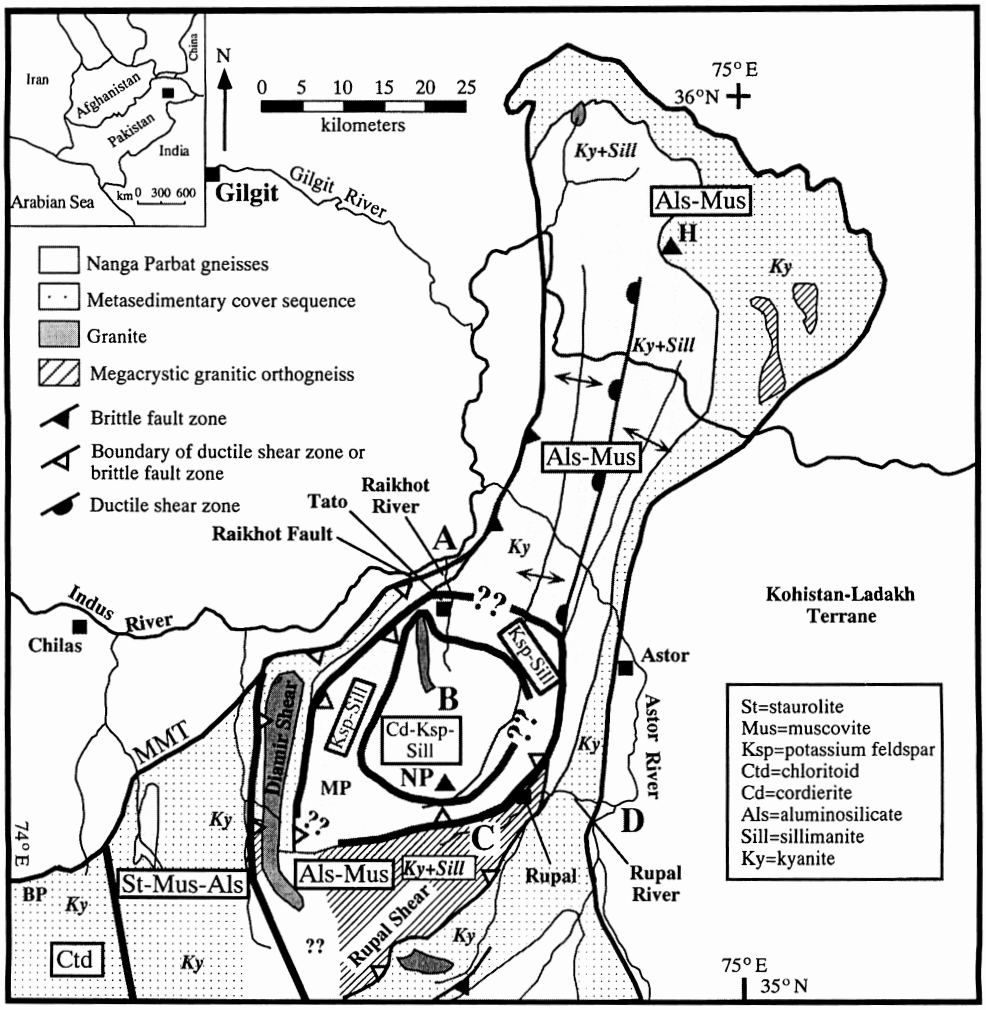


Fig. 1. Geologic and structural map of the Nanga Parbat-Haramosh massif (from Schneider and others, 1999). Heavy lines demarcate the approximate metamorphic mineral assemblage boundaries between chloritoid bearing rocks near Babusar Pass, staurolite bearing rocks between Babusar Pass and the Diamir Shear Zone, aluminosilicate-muscovite rocks over the bulk of the massif, and potassium feldspar-sillimanite and potassium feldspar-cordierite-sillimanite rocks in the massif core. NP=Nanga Parbat summit, H=Haramosh summit, BP=Babusar Pass, MP=Mazeno Pass, MMT=Main Mantle Thrust. A-B and C-D denote end points of the fluid inclusion and oxygen isotope transect across the massif (also see fig. 4).

low and others, 1994; Meltzer and others, ms), active hydrothermal systems (Chamberlain and others, 1995), and multiple episodes of metamorphism have made the NPHM a focal point of active tectonics research.

Rocks within the massif are dominated by high-grade gneisses (referred to here as Nanga Parbat gneisses) and migmatites forming the bulk of the massif, surrounded by a relatively thin cover sequence of metasedimentary rocks (fig. 1). The Nanga Parbat gneisses are accompanied by several generations of anatectic granites (Gazis and others, 1998; Whittington, Harris, and Butler, 1999) as well as smaller units of amphibolite, carbonate, and calc-silicates. Once thought to be equivalent to the High Himalayan Crystalline Series rocks, a recent neodymium isotope study suggests that the gneisses of the massif core are the equivalent of Lesser Himalayan rocks, whereas the metasedimentary cover sequence rocks share geochemical affinities with High Himalayan Crystalline rocks (Whittington and others, 1999).

Structurally, the massif is broadly antiformal with a north-northeast trend and bounded on all sides by the MMT demarcating the boundary between the Indian plate rocks and Ladakh/Kohistan rocks. The exception to this is along the northwestern margin near the Indus River, where the presently active Raikhot Fault system thrusts high-grade metamorphic rocks of the massif over top of Holocene sediments (Butler and Prior, 1988; Butler, Prior, and Knipe, 1989). The structural evolution of the NPHM has been debated with interpretations suggesting that uplift of the massif has resulted either from tectonic denudation processes similar to a metamorphic core complex (Hubbard, Spencer, and West, 1995) or has been accommodated by high angle thrust faults and shear zones within and along the margin of the massif (Butler and Prior, 1988; Schneider and others, 1999; Edwards and others, in press).

Recent studies suggest that Nanga Parbat is not a Himalayan core complex (Butler, Harris, and Whittington, 1997; Schneider and others, 1999; Butler and others, 2000). Internal to the massif, two principal kilometer-scale ductile shear zones showing a reverse sense of motion, the Rupal Shear and the Diamir Shear (connecting with the Raikhot Fault), have been identified along the west, south, and southeast sides of the massif core (Schneider and others, 1999; fig. 1). Along the eastern margin, there is no evidence for continued brittle deformation along the MMT, and it has been suggested that eastern massif margin represents an upturned portion of the MMT (Schneider and others, 1999). Collectively termed a "pop-up structure," the Rupal Shear and the Diamir Shear appear structurally to accommodate west-northwest shortening resulting in the uplift of the massif core relative to adjacent cover sequence rocks, Ladakh/Kohistan rocks and other Nanga Parbat gneisses distal from the massif core (Schneider and others, 1999).

Numerous geochronological studies have been conducted across the massif, consistently showing cooling ages of $<\sim$10 Ma in the core of the massif with older ages toward the massif margins (Zeitler, 1985; Smith, Chamberlain, and Zeitler, 1992; Zeitler, Chamberlain, and Smith, 1993; Winslow, Chamberlain, and Zeitler, 1995). Most recently, Schneider and others (1999) compiled over 200 $^{40}Ar/^{39}Ar$ total fusion biotite ages from the massif south of the Indus River. Recognizing the limitations of total fusion biotite ages, cooling ages are less than 10 Ma in the massif core, increasing sharply across the Diamir and Rupal Shear zones to ages generally $\geq\sim$20 Ma. Consistent correlation with other geochronology systems suggests this is not a result of localized excess argon affecting apparent biotite ages. Cooling ages in the metasedimentary cover sequence rocks toward Babusar Pass (fig. 1) are as old as $\sim$35 Ma, whereas cover sequence rocks along the eastern margin are $\sim$25 to 30 Ma. The steep cooling age gradients across the shear zones suggest that the shear zones define the geographic limits of the massif affected by the most recent tectonism.

The timing of metamorphism at the NPHM is a matter of current debate, in part because the criteria used to define a metamorphic event do not necessarily occur at the same time as ages given by thermochronometers. The NPHM is clearly a polymetamorphic terrane, and there is significant geochronologic, petrologic, and structural evidence for at least three major metamorphic events affecting rocks in and around the massif. Treloar, Wheeler, and Potts (1994) and Wheeler, Treloar, and Potts (1995) suggest that metamorphism responsible for generating the present fabric of the Nanga Parbat gneisses predates the Himalayan orogen. In addition, just to the south of the massif, in the Babusar Pass area, the metamorphic rocks record Himalayan P-T paths (~45 Ma) (Chamberlain, Zeitler, and Erickson 1991). In contrast, Smith, Chamberlain, and Zeitler (1992) and Zeitler, Chamberlain, and Smith (1993) concluded that the high-grade metamorphism in the core of the NPHM is much younger (<10 Ma).

Isotopic and fluid inclusion data suggest the presence of a dual hydrothermal system at Nanga Parbat, consisting of a shallow-level meteoric-dominated system and a deeper level system involving highly rock-exchanged fluids (Chamberlain and others, 1995). Evidence for the shallow system consists of: (1) Hot springs located along faults bordering the massif. These hot spring waters are meteoric in origin (Chamberlain and others, 1995) yet are highly saline suggesting significant water/rock interaction (Gazis and others, 1998). (2) Low $\delta^{18}O$ whole-rock and mineral values in rocks from fault zones as well as some of the granites within the core of the massif (Chamberlain and others, 1995), suggesting that meteoric fluids have extensively interacted with hot rocks at depth within the faults and to a minor extent with the granites in the core of the massif. (3) Abundant secondary calcite veins and disseminated calcite in high-grade granitic gneisses within the core of the massif. Strontium isotopic analyses of these veins (Blum and others, 1998) suggest that they formed from precipitation from a fluid that interacted with the gneisses after high-grade metamorphism in the last 5 Ma at temperatures between 300° and 600°C (Gazis and others, 1998). (4) Fluid inclusion studies show that late-stage fluids moving through fractures were dominantly water with minor $CO_2$ and dissolved salts, and that these fluids were boiling at up to ~400°C (Craw and others, 1994).

Evidence for a deeper hydrothermal system includes: (1) Oxygen isotope studies of quartz veins in high-grade gneisses which show that they formed from highly exchanged fluids (Chamberlain and others, 1995; Craw and others, 1997). (2) Primary fluid inclusions in these quartz veins are commonly dry steam with a variety of compositions from low salinity brine (up to 5 wt percent NaCl equivalent) to water with up to 22 mole percent $CO_2$, and these fluids are thought to have resulted from upward migration of high-temperature (>420°C) low-pressure (<200 bars) supercritical fluid in rock of very low permeability (Craw and others, 1997). (3) Fluid inclusions from high-grade gneisses are commonly rich in carbon dioxide (Winslow and others, 1994). (4) Detrital zircons from gneisses have young (6-11 Ma) U-rich rims, presumably formed from magmatic/metamorphic fluids (Zeitler, Chamberlain, and Smith, 1993; Chamberlain and others, 1995).

In addition, during the last 10 Ma, the NPHM has undergone partial melting and been intruded by leucogranites (<1 percent of rocks exposed), both in the presence and absence of water. These leucogranite stocks and dikes formed in water-undersaturated conditions (Butler, Harris, and Whittington, 1997), presumably as a result of melting of relatively dry rocks during the recent rapid decompression (Zeitler and Chamberlain, 1991), and formed from the melting of rocks not presently exposed in the NPHM (Gazis and others, 1998). Within the core of the massif are cordierite-bearing, granitic veins and migmatites which formed as partial melts during the recent low-pressure high-temperature metamorphism. These veins and migmatites formed under water-saturated conditions (Zeitler, Chamberlain, and Smith, 1993; Butler, Harris, and Whittington,

1997; Whittington, Harris, and Butler, 1999), presumably as a result of the infiltration of metamorphic/magmatic or highly exchanged meteoric fluids (Chamberlain and others, 1995).

## SAMPLES AND ANALYTICAL TECHNIQUES

*Petrography and thermobarometry.*–In the summers of 1995, 1996, and 1997, as part of the larger Continental Dynamics study of Nanga Parbat, we and others collected pelitic schists and gneisses and quartz veins from throughout the massif (fig. 1). To generate the mineral assemblage distribution map shown in figure 1, we examined over 150 thin sections of Nanga Parbat gneisses and cover sequence rocks distributed over most of the massif. In addition, we compiled information from numerous previous studies. Coverage from the Babusar Pass region to the southwest is from Chamberlain, Jan, and Zeitler (1989) and Chamberlain, Zeitler, and Erickson (1991); coverage from the Indus River transect across the massif is from Wheeler, Treloar, and Potts (1995) and Khattak (1995). Additional information is from Misch (1964), Pognante, Benna, and Le Fort (1993), Zeitler, Chamberlain, and Smith (1993), Winslow, Chamberlain, and Zeitler (1995), and Whittington, Harris, and Baker (1998).

A subset of 18 samples of highly aluminous metapelites with appropriate mineralogies and showing textural equilibrium and minimal retrogradation was selected for thermobarometric calculations. Equilibrium mineral assemblages for these samples are compiled in table 1. Microprobe analysis of specific mineral phases for thermobarometry was carried out using Harvard University's Cameca electron microprobe, with an accelerating potential of 15kV and a beam current of 15nA. Conversion from X-ray intensities to wt-percent oxides is as per Bence and Albee (1968). Metamorphic pressure and temperatures were estimated by simultaneous solution of Ferry and Spear's (1978) garnet-biotite geothermometer using the garnet activity model of Hodges and Spear

TABLE 1

*Pressure-temperature estimates and mineral assemblages*

| Sample | Mineral Assemblage | Pressure (kb) and Temperature (°C) Data |
|---|---|---|
| TK 161 | Qtz-Gt-Bio-Musc-Plag-Ky | 8.4, 665 ; 7.6, 650 ; 7.8, 700 |
| SK 492 | Qtz-Gt-Bio-Musc-Plag-Ky | 9.0, 695 ; 11.8, 705 |
| TK 138 | Qtz-Gt-Bio-Musc-Plag-Ky-Tour | 8.3, 580 ; 8.1, 565 ; 7.7, 580 ; 8.5, 635 |
| TK 158 | Qtz-Gt-Bio-Musc-Plag-Ky | 6.6, 569 ; 8.6, 670 |
| 610/10A | Qtz-Gt-Bio-Musc-Ksp-Plag-Ky | 8.2, 535 ; 9.0, 575 ; 7.9, 510 |
| 610/10C | Qtz-Gt-Bio-Musc-Plag-Ky-Sill | 8.4*, 590 |
| 5/27B | Qtz-Gt-Bio-Musc-Plag-Ky?-Tour | 7.8, 590 ; 7.6, 590 |
| AS-3 | Qtz-Gt-Bio-Plag-Ksp-Ky-Tour | 8.0, 575 ; 7.7, 540 |
| AS-E | Qtz-Gt-Bio-Musc-Plag-Ky-Tour | 9.0, 565 ; 10.6, 655 |
| 5/30B | Qtz-Gt-Bio-Musc-Plag-Ky | 11.3, 680 ; 11.3, 695 ; 11.3, 675 |
| 5/29B | Qtz-Gt-Bio-Musc-Plag-Ky | 12.2, 670 ; 11.7, 675 |
| 5/29F | Qtz-Gt-Bio-Plag-Ky-Chl | 13.2, 720 |
| 79/20A | Qtz-Gt-Bio-Musc-Plag-St-Ky-Chl | 6.7, 640 ; 4.6, 550 ; 5.5, 710 |
| 79/21D | Qtz-Gt-Bio-Musc-Plag-Ky | 14.2, 800 |
| FNS-1 | Qtz-Gt-Bio-Musc-Plag-Ky-St | 10.2, 595 |
| FNS-2 | Qtz-Gt-Bio-Plag-Sill-Ky-Chl | 6.5, 535 ; 6.0, 500 ; 8.4, 530 ; 7.6, 500 ; 9.3, 610 |
| TTS-15A | Qtz-Gt-Bio-Musc-Plag-Ky | 10.5, 685 ; 8.3, 595 ; 9.8, 630 |
| TTS-15B | Qtz-Gt-Bio-Musc-Plag-Ky | 9.5, 605 |

Qtz = quartz; Gt = garnet; Bio = biotite; Musc = muscovite; Plag = plagioclase; Ksp = potassium fledspar; Ky = kyanite; Sill = sillimanite; Tour = tourmaline; Chl = chlorite; St = staurolite.
* Pressure assumed to be 8.4 kb due to proximity to sample 610/10A.

(1982) and Newton and Haselton's (1981) garnet-aluminosilicate-plagioclase geobarometer (table 1; fig. 2). Thermobarometric estimates based on rim-rim analyses of touching mineral grains are assumed to be final equilibration temperatures and pressures. Each mineral composition used for P-T calculations represents the average of 1 to 3 analyses of the same mineral along a grain boundary. Each P-T point plotted on figure 2 represents the average of 1 to 5 individual P-T calculations based on analyses of garnet, biotite, and plagioclase coexisting with aluminosilicate and quartz within a single sample. Also shown on figure 2 are additional P-T data compiled from the literature. Figure 3 shows a compilation of published P-T paths interpreted from inclusion mineralogy and Gibbs method calculations.

For purposes of comparison between samples, we chose to use a single thermobarometric calibration, and, wherever possible, samples compiled from the literature were

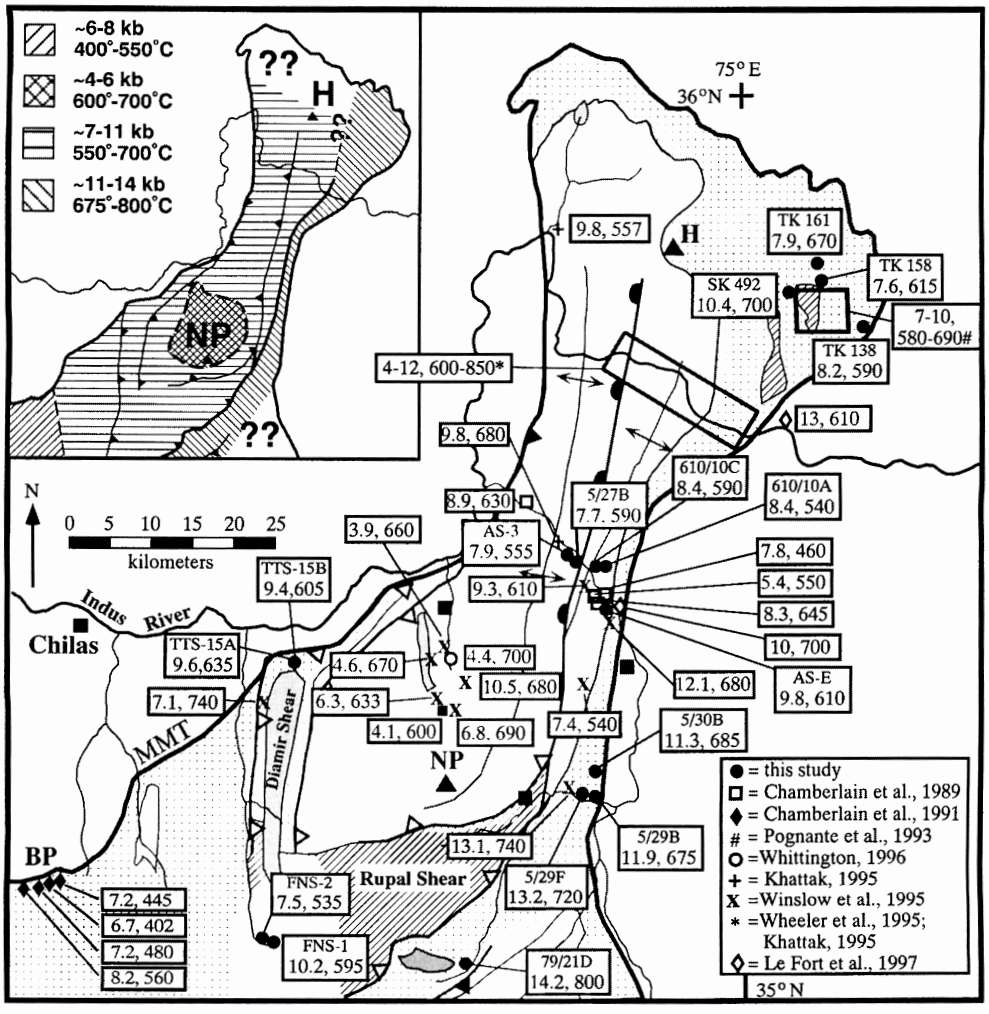


Fig. 2. Compiled map of rim-rim thermobarometry data over the entire NPHM. Patterns and abbreviations are as in figure 1. Solid circles with a sample number are from this study. The data roughly outline the four P-T zones within the massif shown in the inset.

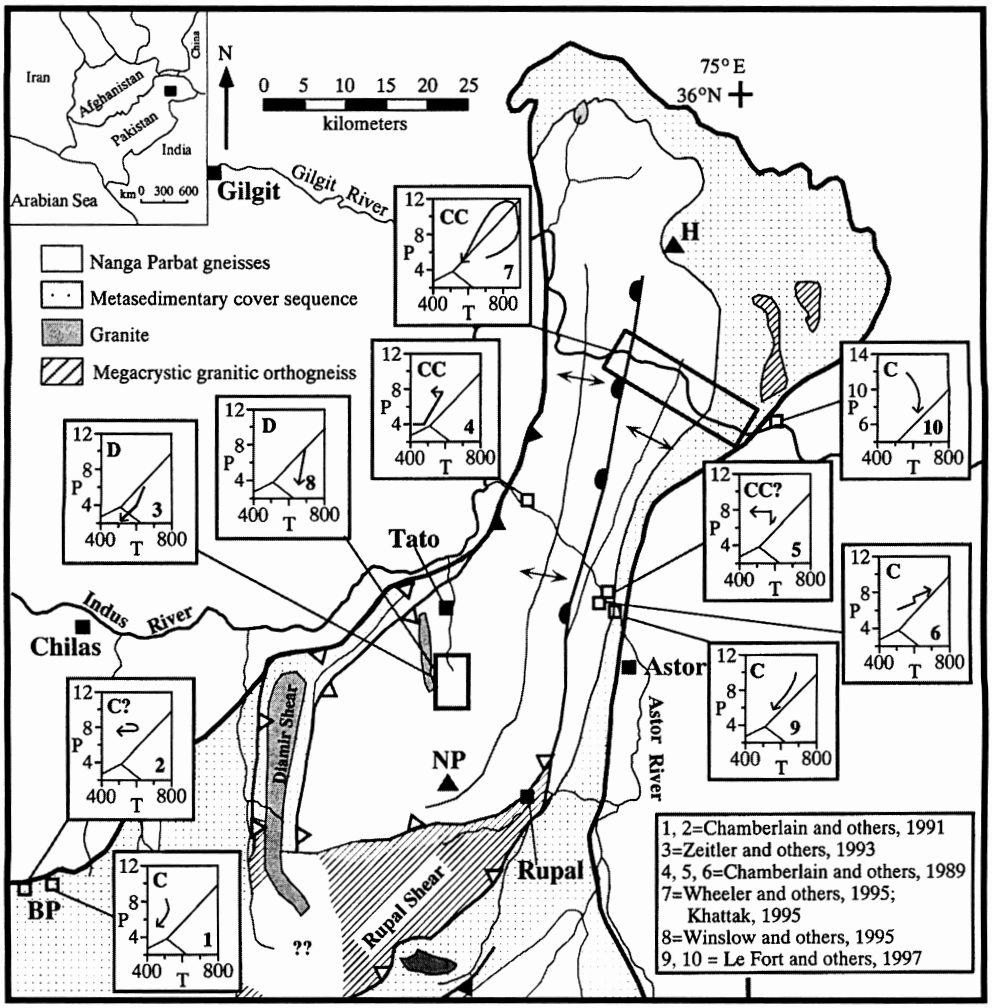


Fig. 3. Map of compiled P-T paths over the entire NPHM. Patterns and abbreviations are as in figure1. The aluminosilicate phase boundaries are shown for reference on each P-T diagram. Most P-T paths are derived from core-rim thermobarometric calculations on common metapelitic minerals. Numbers 9 and 10 (Le Fort, Guillot, and Pêcher, 1997) are calculated from the aluminum content of hornblende and the jadeite content of clinopyroxene, respectively. Bold numbers in the lower right corner of each P-T diagram refer to references listed in the inset. C=clockwise P-T path; CC=counterclockwise P-T path; D=decompressional P-T path.

recalculated using these calibrations. Whereas we recognize the inherent accuracy and precision limitations of thermobarometry (Hodges and McKenna, 1987), we point out that we are primarily interested in broadly delineating spatial zones of different final equilibration metamorphic temperatures and pressures within the massif. As such, we are less concerned with the details of any specific P-T data point or P-T path and omit from our discussion petrographic and geochemical details often accompanying thermodynamically derived P-T estimates.

*Fluid inclusions and oxygen isotopes.*–Quartz veins from the Raikhot Valley (fig. 1, transect A-B) have been studied in detail isotopically and microthermometrically previously (Craw and others, 1994, 1997). To provide two dimensional coverage of the

main massif, we have extended our sampling of quartz veins across the massif along the Rupal River and into the Ladakh amphibolites to the east (fig. 1, transect C-D). All the quartz veins we studied post-date the main metamorphic fabric and fill brittle extensional sites from 1 cm to 1 m across and up to 5 m long. Veins nearest the Raikhot Fault (fig. 1) have been ductilely deformed and fully annealed, and veins from adjacent to the Rupal Shear Zone have been boudinaged and have some quartz recrystallization around their margins. Other veins are undeformed and consist of primary anhedral or prismatic quartz. The veins commonly also contain tourmaline, muscovite, and biotite as accessory minerals, particularly on their margins. Two vein samples were taken from debris derived from the Rupal Face of Nanga Parbat at the head of the Rupal Valley (fig. 1). While these samples were not taken from outcrop, they are undoubtedly from the core of the massif, and the range of outcrops from which they could have been derived is limited, so their marked position southeast of S. Chongra Peak on the cross section (fig. 4) is considered adequate for the scale of this study.

The present study extends the work of Craw and others (1994, 1997) by examining the spatial distribution of different types and compositions of fluid inclusions from quartz veins and host gneisses. Fluid inclusion compositions were determined petrographically with microthermometric calibration using P-V-T-X model calculations in MacFlinCor (Brown and Hagemann, 1995). Salinities of water-rich inclusions were calculated from ice-melting temperatures. Compositions of mixed $H_2O$-$CO_2$ inclusions were calculated by MacFlinCor using microthermometric measurements, and estimates of relative proportions of water-rich and $CO_2$-rich phases are from estimation charts in Roedder (1984). From these primarily petrographic observations, we assigned each generation of fluid inclusions in a sample to a petrographic type (see below), mainly according to distinctive endmember compositions previously described (Craw and others, 1994, 1997; Winslow and others, 1994). Generalized depth zones in which each fluid type occurs are delineated from the relative order of fluid entrapment and estimates of pressure and temperature of entrapment.

For oxygen isotope analyses of these quartz veins, we powdered and homogenized up to 2 g of quartz vein material using either a shatterbox or mortar and pestle. Oxygen was extracted from 10 to 20 mg splits using methods modified from Clayton and Mayeda (1963) and analyzed on either the Finnegan Delta E or Finnegan MAT 252 gas-source mass spectrometer at Dartmouth College. Data are reported relative to V-SMOW using the standard delta notation. Precision is estimated to be $\pm 0.2$ permil based on repeated analysis of the NBS-28 quartz standard as well as an internal laboratory standard. Sample locations, host rocks, and oxygen isotope data for quartz veins from both the Raikhot and Rupal sections are presented in table 2. New fluid inclusion data from quartz veins from the Rupal Section are presented in table 3.

## RESULTS AND INTERPRETATION

*Metamorphic mineral assemblages.*–Based on our analyses of approx 150 thin sections of metapelitic rocks in the massif, we define and constrain the spatial extent of five principle metamorphic zones (fig. 1). These are: (1) chloritoid bearing rocks in the vicinity of Babusar Pass, (2) staurolite bearing rocks to the east of Babusar Pass and west of the Diamir Shear Zone, (3) muscovite-aluminosilicate bearing assemblages over the bulk of the massif, (4) sillimanite-potassium feldspar bearing rocks approaching the massif core, and (5) sillimanite-potassium feldspar-cordierite bearing rocks at the center of the massif core. Each of these metamorphic zones also contains garnet-biotite-quartz-plagioclase and minor amounts of ilmenite and graphite. In most cases, micas, quartz ribbons, and either kyanite or sillimanite define the dominant foliation in both the cover sequence rocks and Nanga Parbat gneisses. Garnets often show spiral inclusion trails of quartz, feldspar, and micas and occasionally show an outer rim of post-kinematic growth.

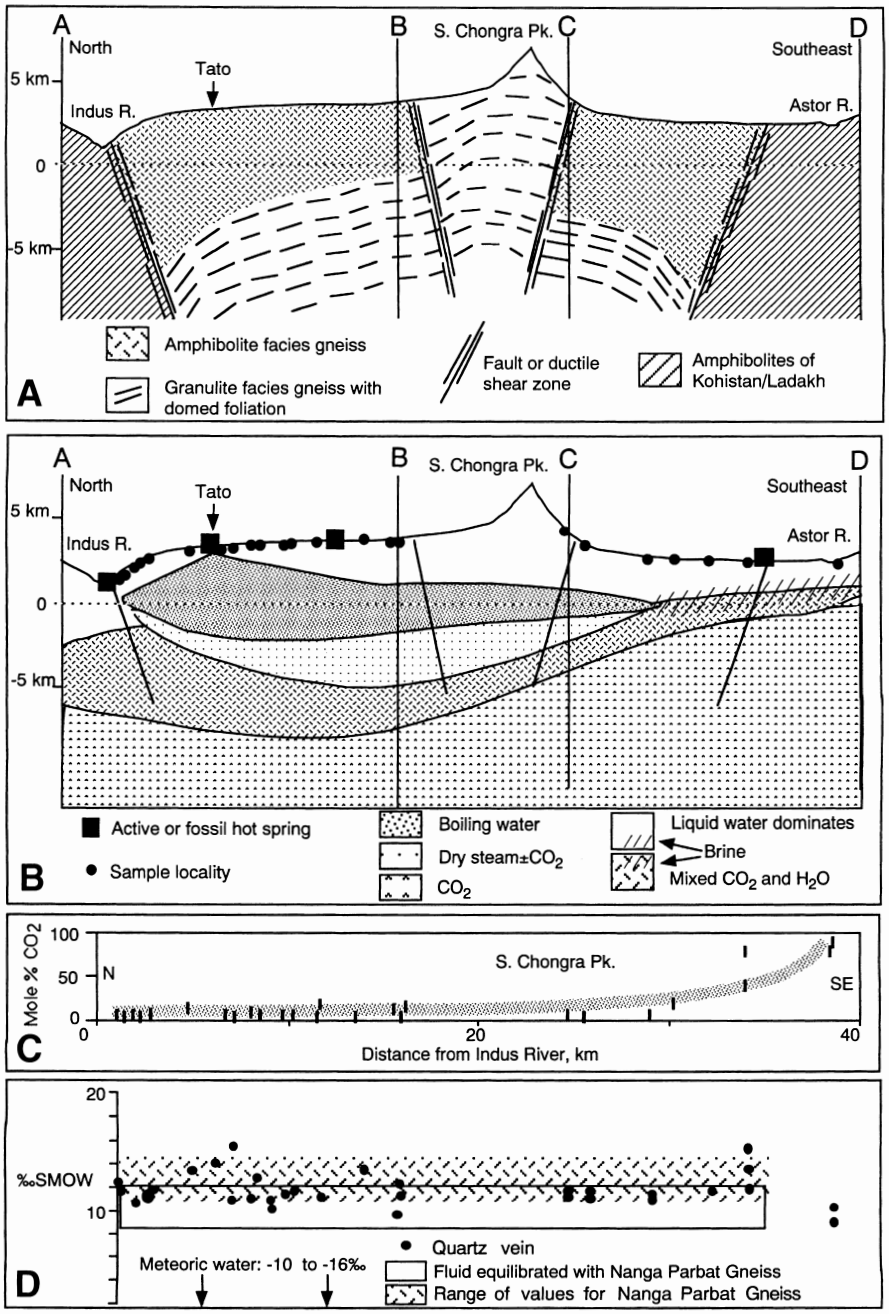


Fig. 4. Cross sections along the transects A-B and C-D shown in figure 1.(A) Generalized lithologic and structural cross section across the core of the massif. (B) Subsurface distribution of fluid compositions based on fluid inclusion data. (C) Mole % $CO_2$ in fluid inclusions across the massif showing a dramatic increase in $CO_2$ content toward the eastern massif margin. (D) Oxygen isotope values from quartz veins showing that fluids quickly isotopically equilibrate with wall rocks, indicating low fluid-rock ratios.

TABLE 2

*Locations and oxygen isotope data for quartz veins*

| Sample | Host | $\delta^{18}O$ (‰) | km. from Indus |
|---|---|---|---|
| ***Raikhot Section (A-B)*** | | | |
| PK112b-90 | gneiss | 12.5 | 0.8 |
| PK99b-90 | gneiss | 11.8 | 1 |
| PK82c-90 | gneiss | 11.0 | 2 |
| PK63b-90 | gneiss | 11.5 | 3 |
| PK8 | gneiss | 13.7 | 5.5 |
| PK404c-92 | sheared gneiss | 14.3 | 7 |
| PK63f-90 | leucogranite | 15.6 | 8 |
| PK9 | gneiss | 11.1 | 8 |
| PK13f-92 | leucogranite | 11.1 | 9.2 |
| PK132a,b-92 | leucogranite | 11.8 | 9.5 |
| PK195b-92 | gneiss | 13.0 | 9.5 |
| PK107b-92 | gneiss | 10.9 | 10.9 |
| PK23 | leucogranite | 10.4 | 11 |
| PK121d-92 | gneiss | 11.2 | 11.2 |
| PK36c-90 | leucogranite | 11.4 | 11.5 |
| PK12 | leucogranite | 13.9 | 13 |
| PK17 | gneiss | 12.4; 11.4 | 17.7 |
| PK18 | leucogranite | 9.6 | 17.5 |
| ***Rupal Section (C-D)*** | | | |
| AS 7a | gneiss | 11.7 | 28.8 |
| AS 7b | gneiss | 11.6 | 28.8 |
| AS 5 | gneiss | 11.4 | 32.5 |
| AS 6 | gneiss | 10.9 | 32.5 |
| AS 8 | gneiss | 10.3 | 34 |
| AS 10 | gneiss | 11.7 | 36 |
| AS 9 | gneiss | 11.7 | 36 |
| AS 3 | gneiss | 13.5 | 38.3 |
| AS 2 | gneiss | 15.3 | 38.3 |
| AS 11 | gneiss | 11.7 | 38.3 |
| AS 1 | amphibolite | 8.7 | 43.6 |
| AS 12 | amphibolite | 10.1 | 43.6 |

Microstructural details of major lithologies within the massif are summarized in Edwards and others (in press).

Chloritoid bearing cover-sequence rocks in the Babusar Pass region have been studied and desscribed extensively by Chamberlain, Jan, and Zeitler (1989) and are the lowest grade rocks exposed at Nanga Parbat. Eastward toward the Diamir Shear Zone, chloritoid-bearing rocks give way to staurolite-kyanite-muscovite bearing rocks. The boundary between the chloritoid and staurolite bearing assemblages is not well constrained, but in the absence of a major unmapped structure, we can only assume that the metasedimentary cover sequence is continuous across this region (fig. 1). East of the Diamir Shear Zone, staurolite is absent, and amphibolite grade rocks contain the

TABLE 3

*Summary fluid inclusion data for the Rupal section*

| Sample | Texture | Homog. to: | $T_h(CO_2)$ | $T_m$(NaCl) | $T_h$(final) | $T_m$(ice/ clathrate) | Mole% $CO_2$ |
|---|---|---|---|---|---|---|---|
| AS 7a | primary | vapor | | | 385-396 | -3.2±0.2 | 0 |
| | secondary | liquid | | | 276-298 | -1.4±0.3 | 0 |
| AS 7b | primary | vapor | | | 378-408 | -2.9±0.3 | 0 |
| | secondary | liquid | | | 248-286 | -1.6±0.2 | 0 |
| AS 5 | primary | vapor | 14-19 | | 328-355 | +7.8±0.3 | 20 |
| | secondary | liquid | | | 240-320 | -1.9±0.5 | 0 |
| AS 6 | primary | vapor | 16-24 | | 338-360 | +7.7±0.3 | 10 |
| | secondary | liquid | | | 264-290 | -2.1±0.2 | 0 |
| AS 8 | primary | vapor | 14-18 | | 340-368 | +7.2±0.3 | 20 |
| | secondary | liquid | | 240-262 | 285-298 | -20 | 0 |
| | secondary | liquid | | | 194-244 | -1.3±0.4 | 0 |
| AS 10 | primary | liquid | 5-8 | | NR | NR | 90 |
| | secondary | liquid | 12-16 | | 330-360 | +7.5±0.5 | 60 |
| | secondary | liquid | | 250-255 | 264-278 | -20 | 0 |
| | secondary | liquid | | | 185-260 | -1.0±0.6 | 0 |
| AS 9 | primary | liquid | 2-8 | | 330-350 | +7.1±0.2 | 60 |
| | secondary | vapor | 0-8 | | NR | NR | 80 |
| | secondary | liquid | | | 190-245 | -1.8±0.4 | 0 |
| AS 3 | primary | liquid | 0-6 | | NR | NR | 90 |
| | secondary | liquid | | 246-256 | 268-292 | -20 | 0 |
| | secondary | liquid | | | 205-248 | -1.4±0.3 | 0 |
| AS 2 | primary | liquid | 15-21 | | 362-380 | -2.5±0.3 | 60 |
| | secondary | liquid | | | 294-305 | -3.1±0.4 | 0 |
| AS 11 | primary | liquid | 0-6 | | NR | NR | 90 |
| | secondary | liquid | | 245-250 | 255-260 | -20 | 0 |
| | secondary | liquid | | | 185-228 | -0.9±0.3 | 0 |
| AS 1 | secondary | liquid | 3-8 | | NR | NR | 90-100 |
| AS 12 | secondary | liquid | 0-6 | | NR | NR | 90-100 |

Notes: Columns show, in order: Sample number (see table 2 for location and host); primary or secondary inclusion texture (see Roedder, 1984); phase to which inclusions finally homogenize; carbon dioxide homogenization temperature (°C); cubic daughter crystal final dissolution temperature (°C); final homogenization temperature (°C); ice or clathrate melting temperature (°C); and estimated mole % carbon dioxide content (see text). NR denotes water phase was not resolvable.

assemblage quartz-muscovite-biotite-garnet-plagioclase±kyanite±sillimanite, with the dominant aluminosilicate phase indicated in figure 1. The bulk of the metapelitic Nanga Parbat gneisses from the Astor River north contain similar Al-silicate and muscovite bearing assemblages. Approaching the Nanga Parbat summit, a narrow zone of potassium feldspar-sillimanite bearing rocks gives way to cordierite-potassium feldspar-sillimanite assemblages stable in the massif core. This granulite grade assemblage is accompanied by anatectic cordierite-bearing granitic veins indicating metamorphic conditions at or near the granite solidus. Cordierite bearing rocks in the Raikhot Valley north of Nanga Parbat as well as cordierite-bearing float observed in the Rupal Valley southeast of Nanga Parbat suggest that the summit region is in the cordierite-potassium feldspar-sillimanite zone. Based on our analysis of mineral assemblages in outcrops and float from valleys, it is apparent that the upper amphibolite and granulite mineral

assemblage boundaries must be somewhat concentric around the summit of Nanga Parbat.

Spatial accuracy of the assemblage boundaries depends largely on local accessibility and sampling density. For example, the boundary between chloritoid and staurolite bearing assemblages in the southwest quadrant of figure 1 is an approximate boundary, constrained only by the samples of Chamberlain, Jan, and Zeitler (1989) to the west and samples from this study 25 km to the east. The eastern limit of the staurolite-muscovite-Al-silicate assemblage is better constrained to the north, where sample coverage is denser and less well constrained to the south, where coverage is relatively poor. The positions of the potassium feldspar-sillimanite and cordierite-sillimanite-potassium feldspar curves shown in figure 1 are better constrained to the north and west due to access up the Raikhot Valley and over Mazeno Pass.

Several mineral assemblage boundaries, particularly toward the massif core, are roughly coincident with major structures internal to the massif suggesting that these boundaries may represent structurally controlled juxtaposition of different grade metamorphic rocks rather than true metamorphic isograds. For example, the boundary between staurolite-bearing and staurolite-absent rocks appears roughly coincident with the Diamir Shear Zone and, coupled with steep cooling-age gradients across the shear (Schneider and others, 1999), suggests that shear zone displacement may contribute to the overall steep metamorphic field gradient observed between Nanga Parbat summit and Babusar Pass. Microstructural analyses of rocks across the Diamir Shear Zone indicating synkinematic recrystallization of metamorphic minerals in the shear zone is summarized in Edwards and others (in press).

*Thermobarometry.*–Figure 2 shows new thermobarometric pressure-temperature analyses (table 1) of highly aluminous pelitic rocks compiled with data from previous studies (Chamberlain, Jan, and Zeitler, 1989; Chamberlain, Zeitler, and Erickson, 1991; Pognante, Benna, and Le Fort, 1993; Zeitler, Chamberlain, and Smith, 1993; Khattak, 1995; Wheeler, Treloar, and Potts, 1995; Winslow, Chamberlain, and Zeitler, 1995; Whittington, 1996; Le Fort, Guillot, and Pêcher, 1997; Whittington, Harris, and Baker, 1998). The data outline four distinct and generally continuous final equilibration pressure-temperature zones within the massif (fig. 2, inset).

Near Babusar Pass P-T data from cover sequence rocks show that final equilibration occurred at moderate pressures and relatively low temperatures (~6-8 kb, 400°-550°C, Chamberlain, Zeitler, and Erickson, 1991), roughly consistent with the observed chloritoid-bearing mineral assemblages. The bulk of the Nanga Parbat gneisses (exclusive of the massif core) have higher temperatures and pressures in the vicinity of ~7 to 11 kb and 550° to 700°C. The core of the massif is characterized by distinctly lower pressures but equally high temperatures (~4-6 kb, 600°-700°C). The eastern margin cover sequence is characterized by high pressures and temperatures (~11-4 kb, 675°-800°C) and is consistent with eclogite facies rocks immediately adjacent to the massif (Le Fort, Guillot, and Pêcher, 1997). The boundaries of these regions are not well constrained due to low sample density, but some appear roughly coincident with major mineral assemblage boundaries, faults, and/or lithologic contacts.

Compiled published P-T paths (Chamberlain, Jan, and Zeitler, 1989; Chamberlain, Zeitler, and Erickson, 1991; Zeitler, Chamberlain, and Smith, 1993; Khattak, 1995; Wheeler, Treloar, and Potts, 1995; Winslow, Chamberlain, and Zeitler, 1995; Le Fort, Guillot, and Pêcher, 1997) suggest three general P-T histories interpreted from NPHM rocks. First, rocks along the flanks of the massif, in particular in the Babusar Pass region and the eastern massif margin, generally record retrograde fragments of clockwise P-T paths, with the eastern margin rocks originating at relatively high-pressures (Chamberlain, Jan, and Zeitler, 1989; Pognante, Benna, and Le Fort, 1993; Le Fort, Guillot, and Pêcher, 1997; labeled C in fig. 3). Second, some of the Nanga Parbat gneisses in the

interior of the massif, particularly along the Astor and Indus Rivers generally show elements of counter-clockwise P-T paths (Chamberlain, Jan, and Zeitler, 1989; Wheeler, Treloar, and Potts, 1995; Khattak, 1995; labeled CC in fig. 3). Third, rocks in the core of the massif generally show low-pressure, near-isothermal decompression P-T paths (Zeitler, Chamberlain, and Smith, 1993; Winslow, Chamberlain, and Zeitler, 1995; labeled D in fig. 3).

Without geochronological information on the early portion of a rock's P-T history it is difficult to assign a particular P-T trajectory to a specific tectonic event. However, given the current understanding of the structural history of Nanga Parbat (Schneider and others, 1999), it is possible to place some constraints on the origin of the three P-T paths discussed above. The decompression P-T path (labeled D in fig. 3) in the massif core is the best constrained trajectory, because of high-temperature geochronological results demonstrating young metamorphism (< 10 Ma) (Zeitler, Chamberlain, and Smith, 1993), the occurrence of decompression melts (Winslow, Chamberlain, and Zeitler, 1995; Whittington, Harris, and Baker, 1998), and the presence of low-pressure, high-temperature mineral assemblages (Zeitler, Chamberlain, and Smith, 1993; Whittington, Harris, and Baker, 1998). These P-T paths reflect the recent rapid uplift/exhumation of the massif core along the bounding faults and shear zones that create this pop-up structure.

The origin of the clockwise and counter-clockwise P-T paths is, however, less certain as P-T paths can vary widely within a single metamorphic terrane (Chamberlain and Karabinos, 1987), especially those characterized by complex deformational histories. The counter-clockwise P-T paths (labeled CC in fig. 3) have been tentatively ascribed to loading and heating of the Indian plate rocks by the overriding Kohistan arc during earlier stages of Himalayan collision (Chamberlain, Jan, and Zeitler, 1989; Khattak, 1995; Winslow, Chamberlain, and Zeitler, 1995), and we have no additional evidence to confirm or refute this view. Geochronological information on mineral inclusions within garnets in these rocks may help to constrain the timing of the early P-T history. The clockwise P-T paths (labeled C in fig. 3) have been ascribed to early subduction of Indian plate rocks and later exhumation of these high-pressure assemblages (Le Fort, Guillot, and Pêcher, 1997). These P-T paths reflect Himalayan metamorphism between approx 50 to 30 Ma (Chamberlain, Zeitler, and Erickson, 1991; Tonarini and others, 1993; Schneider and others, 1999). In this regard, it is interesting to note that these P-T paths occur within both the high-pressure rocks exposed on the east-side of the massif as well as rocks near Babusar Pass. This suggests that these rocks have not been overprinted by either the loading of the Kohistan arc or by the recent deformation and metamorphism centered on the massif core.

*Fluid inclusions.*–Fluid inclusion compositions vary widely across the massif, and distinct zones can be delineated both laterally and with depth. Inclusions trapped nearest the surface over the whole massif are liquid water. These two-phase inclusions are dominated by liquid with subordinate (10-20 v. percent) vapor bubbles. These inclusions homogenize at 240° to 330°C, have low salinity (<2 wt percent NaCl equivalent), and occur only in the latest stages of secondary inclusion trails filling healed fractures cross-cutting most quartz veins. Some samples have several generations of liquid water inclusions, with different homogenization temperatures and slightly differing salinities, but for the purposes of this study these have all been mapped together as the shallowest zone in figure 4.

Coexisting liquid-rich and vapor-rich water inclusions occur in secondary inclusion trails in most samples from the middle and upper Raikhot valley and in the two samples from the Rupal Face. These inclusions are interpreted to have been trapped during boiling, at temperatures between 340° and 390°C, with salinities up to 5 wt percent NaCl equivalent (Craw and others, 1994). Some samples from the same areas have co-existing

two-phase and three-phase inclusions with significant $CO_2$ content (up to 20 mole percent) indicative of fluid immiscibility in the $H_2O$-$CO_2$ system (Craw and others, 1994). All these mixed secondary inclusions are treated as a single group which is spatially restricted to the areas described above.

Many of the veins from the middle and upper Raikhot Valley and the Rupal Face samples, including those with mixed secondary inclusions (previous paragraph), have vapor-rich primary inclusions. These dry steam inclusions have salinities up to 5 wt percent NaCl equivalent and homogenize at temperatures up to 415°C (Craw and others, 1997). Some dry steam inclusions also contain a separate $CO_2$ phase at room temperature, with all inclusions in a single sample, or portion of a sample, having the same composition. In samples where all three inclusion types are present, the dry steam inclusions clearly predate both the boiling and liquid water inclusions described above.

Fluid inclusions in metamorphic minerals in Nanga Parbat gneisses are almost invariably mixtures of low salinity $H_2O$ and $CO_2$, with uniform compositions within each sample or portion of a sample (Winslow and others, 1994). High grade gneisses of the middle and upper Raikhot Valley contain inclusions with $<\sim$35 mole percent $CO_2$, whereas amphibolite facies gneisses of the middle and lower Rupal Valley contain $CO_2$-rich inclusions (typically 80-100 mole percent). Likewise, Ladakh amphibolite gneisses of the Astor Valley (fig. 1) also contain $CO_2$-rich inclusions. Veins in Nanga Parbat and Ladakh gneisses in the middle and lower Astor Valley and southwest of Mazeno Pass contain $CO_2$-rich fluids similar to their host rocks as primary inclusions, with cross-cutting secondary inclusion trails containing $H_2O$-$CO_2$ fluids with 20 to 70 mole percent $CO_2$. Some of the more water-rich of the latter inclusions contain unidentified daughter crystals and have salinities of up to 35 wt percent NaCl equivalent. In all these gneisses there is a clear sequence of decreasing $CO_2$ content in fluid inclusions with decreasing relative age of the inclusions. In addition, there is a distinct lack of vapor-rich inclusions on the margins of the massif as compared to the core. It is important to note that the fluids described above were present in small volumes in sparsely-distributed fractures cutting the rocks, and that most of the rocks contained only minor $CO_2$-rich fluid.

Evidence for boiling fluid beneath the core of the massif helps to constrain fluid pressure and therefore depth of the boiling zone to $\sim$2 to 6 km below surface (Craw and others, 1994). Imprecision is due to the poorly known fluid density structure below the surface. Fluid is locally boiling right to the surface hot springs near Tato (fig. 4), and other hot springs attest to near-surface fluid thermal anomalies. Hence, we have defined a boiling zone near sealevel beneath the massif (fig. 4), locally extending toward the surface. Above this zone, liquid water dominates. The boiling zone may extend as far north as hot springs located near the Indus River but does not extend as far east as the summit region, as the only evidence of boiling in the Astor catchment comes from the two debris samples from the Rupal Face (fig. 4).

A zone with dry steam extends below the boiling zone to the brittle-ductile transition (Craw and others, 1997). This zone is hydrostatically pressured and is inferred to extend almost to the base of seismic activity which is $\sim$5 km below sealevel (Meltzer and others, in review). The lateral extent of the dry steam zone is similar to that of the boiling zone and extends only as far east as the two debris samples from the Rupal Face (fig. 4). Zones with $H_2O$-$CO_2$-bearing fluids, grading down to dominantly $CO_2$ fluid, are shown extending down from the dry steam zone under the massif. These zones extend closer to the surface on most margins of the massif (see southeast end, fig. 4), where they are overprinted only by near-surface liquid water. Brines also occur toward the upper end of the $H_2O$-$CO_2$ bearing zones. The positions of the boundaries in these regions are poorly constrained, but the relative order with depth is robust.

The distribution of fluids shown in figure 4 suggests that surface waters of meteoric origin penetrate locally to below sealevel beneath the massif and migrate toward the massif margins where they discharge as hot springs. Metamorphic fluids, predominantly $CO_2$, are rising from beneath the massif and mix with the downward-percolating surface waters. It is notable that the highest grade (granulite facies) rocks in the massif contain little $CO_2$, and $CO_2$ dominates only on the eastern margin of the massif where radiometric cooling ages are oldest and exhumation estimates slowest (Schneider and others, 1999). This is in strong contrast to most other high grade rocks and their enclosed veins elsewhere in the Himalaya, which typically contain fluids with 80 to 100 percent $CO_2$ (Pêcher, 1979; Craw, 1990). The fact that $CO_2$ dominates only in the region of dominantly Himalayan age metamorphism suggests that downward percolation of meteoric water in the massif core is driven by the presently rapid uplift rates and high topography, consistent with fluid mixing models in active orogenic belts (Koons and Craw, 1991). The source of the brines near the eastern massif margin is not known, but these are common features of amphibolite facies rocks elsewhere in the Himalaya (Pêcher, 1979; Craw, 1990) and most ancient metamorphic belts and are thought to have developed through extreme water-rock interaction (Crawford, Filer, and Wood, 1979).

*Oxygen isotopes.*–Oxygen isotope values ($\delta^{18}O$) of vein quartz range from 8.7 to 15.6 permil, with the majority of the values from 10 to 13 permil (table 2). These values are consistent with measured whole-rock oxygen isotope ratios in Nanga Parbat gneisses which are typically +9 to +12 permil (Chamberlain and others, 1995). The $\delta^{18}O$ values of quartz veins show no significant variation across the bulk of the massif, in contrast to $\delta^{18}O$ whole-rock values are relatively low in shear zones where infiltrating meteoric water ($\delta^{18}O$= -10 to -16 permil) has locally altered the rock (Chamberlain and others, 1995). The two quartz veins in the Ladakh amphibolites have relatively low $\delta^{18}O$ values (8.7 and 10.1 permil), reflecting the typically lower $\delta^{18}O$ values of mafic rocks. Interaction between this meteoric fluid and the rock ultimately causes the fluid to lose its meteoric isotopic signature in the core of the massif (Craw and others, 1997). Hence, while water discharging from active springs retains its meteoric signature (Chamberlain and others, 1995), water that forms quartz veins at depth in the core of the massif has a rock-dominated isotopic signature (Craw and others, 1997).

## DISCUSSION

A recently proposed tectonic model, based on structural mapping and $^{40}Ar/^{39}Ar$ total fusion biotite ages, suggests that the NPHM represents a crustal scale "pop-up structure" (Schneider and others, 1999). In this model, young cooling ages in the center of the massif result from recent and rapid structural and surface uplift and denudation of the massif core, grading outward across active bounding faults and shear zones to Himalayan ages at the eastern massif margin. The new petrologic, fluid inclusion and stable isotopic data presented in this paper together with data from numerous former studies of the massif allow us to evaluate further the pop-up structure model and to place fluid models of the massif (Chamberlain and others, 1995) in a larger-scale context.

With respect to the massif core, our petrologic compilation is consistent with the pop-up structure model of Schneider and others (1999). Specifically, we find: (1) roughly concentric boundaries between metamorphic zones, with the highest-grade assemblages occurring in the core of the massif, (2) metamorphic assemblage breaks occurring approximately along the bounding structures, and (3) low-pressure, high-temperature final equilibration conditions and decompression P-T paths in the high-grade core of the massif. These data, taken together with numerous geochronology studies, suggest that the core of the massif is the locus of highest exhumation and that the bounding faults and shear zones separate the recently deeply exhumed rocks of the core from the surrounding metamorphic rocks.

Also consistent with the pop-up structure model, we suggest that the very core of the massif (that marked by the cordierite-potassium-feldspar assemblages) represents recent metamorphism. We base this conclusion on three pieces of evidence. First, within this metamorphic zone are cordierite-bearing granitic melts that give young U/Pb ages (3-1 Ma) of both zircon (Zeitler, Chamberlain, and Smith, 1993) and monazite (Smith, Chamberlain, and Zeitler, 1992; Zeitler, Chamberlain, and Smith, 1993). Second, these rocks show decompression P-T paths and relatively low pressure-high temperature final equilibration conditions and mineral assemblages, unlike the surrounding metamorphic rocks. Finally, the cordierite-bearing rocks of the massif core are coincident with the youngest cooling ages (see fig. 3 of Schneider and others, 1999).

The young pop-up structure is manifested in the changing P-T paths and timing of metamorphism from the core to the edge of the massif. As discussed above the core of the massif is characterized by young, granulite-grade metamorphism showing decompression P-T paths. In contrast, along the edges of the massif the rocks record the earlier Himalayan tectonic history. For example, our and other studies (Pognante, Benna, and Le Fort, 1993; Le Fort, Guillot, and Pêcher, 1997) have shown that the east margin of the massif consists of metamorphic rocks that equilibrated at relatively high pressures (~10 to 12 kb) and that this high-pressure belt continues well south of the massif (Pognante and Spencer, 1991). In addition, clockwise metamorphic P-T paths from the eastern margin and near Babusar Pass record this early phase of metamorphism. Though the precise age of the early metamorphism is unknown, Nd/Sm eclogite whole-rock ages of the high-pressure rocks are ~49±6 Ma (Tonarini and others, 1993), total fusion $^{40}Ar/^{39}Ar$ biotite ages of the eastern margin of the massif are as old as ~30 Ma (Schneider and others, 1999), and $^{40}Ar/^{39}Ar$ geochronology of hornblendes from Babusar Pass gives ages of ~45 Ma (Chamberlain, Zeitler, and Erickson, 1991).

The development of the pop-up structure also created a unique hydrothermal system within the massif characterized by meteoric and metamorphic fluid mixing within the massif core as well as marked differences in fluid regimes over tens of kilometers between the core and outboard regions. Our fluid inclusion data show two important results with respect to the pop-up structure model. First, within the massif core, fluids are dominantly water-rich and extend down to ~5 km below sealevel, suggesting deep meteoric infiltration. Second, the nature of the fluid changes vertically and horizontally, becoming more $CO_2$-rich both with depth and toward the eastern massif margin (fig. 4).

Rapid uplift and exhumation of the massif core created both steep topographic gradients and uplifted isotherms, allowing for deep meteoric fluid infiltration into the massif and facilitating deep flow of metamorphic and magmatic fluids (Chamberlain and others, 1995). Deep penetration of meteoric fluids as evidenced by water-rich inclusions in the massif core is directly attributable to the rapid tectonic uplift of the massif core. These meteoric fluids then mix with rising metamorphic/magmatic fluids at depth to generate the subsurface fluid distribution shown in figure 4. In contrast to the massif core, quartz veins in rocks along the eastern edge of the massif, those with older cooling ages and inferred Himalayan-age metamorphism, contain dominantly $CO_2$-rich fluid inclusions. We suggest these differences in fluids reflect the different tectonic histories across the massif in accordance with the pop-up structure model. Specifically, along the eastern margin the fluids are relatively old and metamorphic in origin and have not mixed with deeply infiltrating meteoric waters as in the massif core. This is consistent with structural observations showing that the MMT in this region has been upturned but not reactivated by the recent tectonic activity affecting the massif core (Schneider and others, 1999).

A critical question regarding the nature of fluid flow is the quantity of fluids involved. Whereas no one questions that fluids have been present at Nanga Parbat (see earliest work by Misch, 1949), the abundance of fluids may be limited. A recent

magnetotelluric survey (Park and Mackie, 1997) shows little evidence for widespread interconnected fluids. In addition, fluids appear to have isotopically equilibrated with local wallrocks suggesting a rock-dominated system. The lack of strong magnetotelluric conductors underneath the massif and the fact that the quartz veins have equilibrated with the gneisses indicates that, with the exception of the faults (Chamberlain and others, 1995; Butler, Harris, and Whittington, 1997), the hydrothermal system at Nanga Parbat is rock-dominated with low fluid:rock ratios.

## CONCLUSIONS

Our massif-wide petrologic data set is consistent with Nanga Parbat forming as a recent pop-up structure as proposed by Schneider and others (1999). We find that there are distinct and predictable zones of both metamorphic mineral assemblages, final-equilibrated metamorphic pressures and temperatures, and, to a lesser extent, pressure-temperature paths within the massif. The highest grade and lowest pressure rocks are located in the same area as the highest topography, youngest radiometric cooling ages (Schneider and others, 1999) and highest denudation rate estimates in the core of the massif (Zeitler, Chamberlain, and Smith, 1993; Winslow and others, 1994; Whittington, 1996, Schneider and others, 1999) and likely reflect a local upward telescoping of isotherms beneath this rapidly exhuming terrane. Metamorphic grade decreases outward from the core across several young thrust faults and shear zones internal to the massif suggesting that these structures play a significant role in juxtaposing rocks of significantly different metamorphic grade over tens of kilometers. Four distinct zones defined by thermobarometric data include a low pressure-high temperature zone centered around the massif core (~4-6 kb, 600°-700°C), lower temperature rocks at the southwest margin (~6-8 kb, 400°-550°C), intermediate pressures with variable temperatures (~7-11 kb, 550°-700°C) over the bulk of the massif, and a high pressure belt along the eastern massif margin (~11-14 kb, 675°-800°C). Combined with a compilation of P-T paths and recent geochronologic and structural data, we suggest that these petrologic features record earlier Himalayan metamorphism toward the edges of the massif, as well as a younger metamorphic overprint associated with more recent uplift and denudation centered on the massif core.

The present structure and topography of the massif has generated a subsurface distribution of fluid compositions through which all rocks must be uplifted. This fluid distribution pattern can be identified to at least 8 to10 km below the surface and is known to be important down to ~15 to 20 km depth (Park and Mackie, 1997). From a fluid inclusion and oxygen isotopic study of a transect across the massif, we suggest that there are two distinct fluid sources related to the tectonic history. The development of the "pop-up structure" created a dual hydrothermal system fed by downward percolating meteoric water mixing with metamorphic waters at depth. In the region of recent rapid uplift higher level fluids are dominated by meteoric water which has isotopically equilibrated with the rocks indicating low fluid:rock ratios. Conversely, in areas unaffected by recent tectonism the fluid is $CO_2$-rich and metamorphic in origin. These fluids are likely associated with Himalayan-age metamorphism.

## ACKNOWLEDGMENTS

We wish to thank D.A. Schneider, M.A. Edwards, M. Riaz, and P. Le Fort for providing rock samples from throughout the massif. We thank P.O. Koons and P.K. Zeitler for many useful discussions and ideas with respect to this manuscript. The manuscript benefited from thoughtful reviews by Kurt Stüwe and an anonymous reviewer. This research was supported by NSF grant EAR-9418154 to Chamberlain, a NSF Graduate Research Fellowship to Poage, and the University of Otago.

## References


Bence, A.E. and Albee, A.L., 1968, Empirical correction factors of the electron microanalysis of silicates and oxides: Journal of Geology, v. 76, p. 382–403.

Blum, J.D., Gazis, C.A., Jacobson, A.D., and Chamberlain, C.P., 1998, Carbonate versus silicate weathering in the Raikhot watershed within the High Himalayan Crystalline Series: Geology, v. 26, p. 411–414.

Brown, P.E., and Hagemann, S.G., 1995, MacFlinCor and its application to fluids in Archean lode-gold deposits: Geochimica et Cosmochimica Acta, v. 59, p. 3943–3952.

Butler, R.W.H., George, M., Harris, N.B.W., Jones, C., Prior, D.J., Treloar, P.J., and Wheeler, J., 1992, Geology of the northern part of the Nanga Parbat massif, northern Pakistan, and its implications for Himalayan tectonics: Journal of the Geological Society of London, v. 149, p. 557–567.

Butler, R.W.H., Harris, N.B.W., and Whittington, A.G., 1997, Interactions between deformation, magmatism and hydrothermal activity during active crustal thickening: a field example from Nanga Parbat, Pakistan Himalayas: Mineralogical Magazine, v. 61, p. 37–52.

Butler, R.W.H, and Prior, D.J., 1988 Tectonic controls on the uplift of the Nanga Parbat Massif, Pakistan Himalayas: Nature, v. 333, p. 247–250.

Butler, R.W.H., Prior, D.J., and Knipe, R.J., 1989, Neotectonics of the Nanga Parbat syntaxis, Pakistan, and crustal stacking in the northwest Himalayas: Earth and Planetary Science Letters, v. 94, p. 329–343.

Butler, R.W.H., Wheeler, J., Treloar, P.J., and Jones, C., 2000, Geological structure of the southern part of the Nanga Parbat massif, Pakistan Himlaya, and its tectonic implications, *in* Khan, M.A, Treloar, P.J., Searle, M.P., and Jan, M.Q., editors, Geological Society of London Special Publication 170: Tectonics of the Nanga Parbat Syntaxis and the Western Himalaya: Geological Society of London Special Publication 170, p. 123–136.

Chamberlain, C.P., Jan, M.Q., and Zeitler, P.K., 1989, A petrologic record of the collision between the Kohistan Island-Arc and Indian Plate, northwest Himalaya, *in* Malinconico, L.L., and Lillie, R.J., editors, Tectonics of the Western Himalayas: Geological Society of America Special Paper 232, p. 23–32.

Chamberlain, C.P., and Karabinos, P., 1987, Influence of deformation on pressure-temperature paths of metamorphism: Geology, v. 15, p. 42–44.

Chamberlain, C.P., Zeitler, P.K., Barnett, D.E., Winslow, D., Poulson, S.R., Leahy, T., and Hammer, J.E., 1995, Active hydrothermal systems during the recent uplift of Nanga Parbat, Pakistan Himalaya: Journal of Geophysical Research, v. 100, p. 439–453.

Chamberlain, C.P., Zeitler, P.K., and Erickson, E., 1991, Metamorphism at Babusar Pass, northern Pakistan: implications for the metamorphic evolution of the northwest Himalaya: Journal of Petrology, v. 99, p. 829–849.

Clayton, R.N. and Mayeda, T.K., 1963, The use of bromine-pentafluoride in the extraction of oxygen from oxides and silicates for isotopic analysis: Geochimica et Cosmochimica Acta, v. 27, p. 43–52.

Craw, D., 1990, Fluid evolution during uplift of the Annapurna Himal, central Nepal: Lithos, v. 24, p. 137–150.

Craw, D., Chamberlain, C.P., Zeitler, P.K., and Koons, P.O., 1997, Geochemistry of a dry stream geothermal zone formed during rapid uplift of Nanga Parbat, northern Pakistan: Chemical Geology, v. 142, p. 11–22.

Craw, D., Koons, P.O., Winslow, D., Chamberlain, C.P., and Zeitler, P.K., 1994, Boiling fluids in a region of rapid uplift, Nanga Parbat massif, Pakistan: Earth and Planetary Science Letters, v. 128, p. 169–182.

Crawford, M.L., Filer, J., and Wood, C., 1979, Saline fluid inclusions associated with retrograde metamorphism: Bulletin de Mineralogie, v. 102, p. 562–568.

Edwards, M.A., Kidd, W.S.F., Khan, M.A., and Schneider, D.A., in press, Tectonics of the SW margin of the Nanga Parbat-Haramosh Massif: Journal of the Geological Society of London.

Ferry, J.M., and Spear, F.S., 1978, Experimental calibration of the partitioning of Fe and Mg between garnet and biotite: Contributions to Mineralogy and Petrology, v. 66, p. 113–117.

Gazis, C.A., Blum, J.D., Chamberlain, C.P., and Poage, M.A., 1998, Isotope systematics of granites and gneisses on the Nanga Parbat Massif, Pakistan Himalaya: American Journal of Science, v. 298, p. 673–698.

George, M.T., and Bartlett, J.M., 1996, Rejuvenation of Rb-Sr mica ages during shearing on the northwestern margin of the Nanga Parbat-Haramosh massif: Tectonophysics, v. 260, p. 167–185.

Hodges, K.V., and McKenna, L.W., 1987, Realistic propagation of uncertainties in geologic thermobarometry: American Mineralogist, v. 72, p. 671–680.

Hodges, K.V., and Spear, F.S., 1982, Geothermometry, geobarometry and the $Al_2SiO_5$ triple point at Mt. Moosilauke, New Hampshire: American Mineralogist, v. 67, p. 1118–1134.

Hubbard, M.S., Spencer, D.A., and West, D.P., 1995, Tectonic exhumation of the Nanga Parbat massif, northern Pakistan: Earth and Planetary Science Letters, v. 133, p. 213–225.

Khattak, W.U.K., ms, 1995, Petrology and stable isotope geochemistry of the Nanga Parbat-Haramosh massif, northern Pakistan: Ph.D. thesis, University of South Carolina, 158 p.

Koons, P.O., and Craw, D., 1991, Evolution of fluid driving forces and composition within collisional orogens: Geophysical Research Letters, v. 18, p. 935–938.

Le Fort P., Guillot, S., and Pêcher, A., 1997, HP metamorphic belt along the Indus suture zone of NW Himalaya: new discoveries and significance: Comptes Rendus de L'Academie des Sciences, serie II, Sciences de la terre et des planetes, v. 325, p. 773–778.

Misch, P., 1949, Metasomatic granitization of batholithic dimensions: American Journal of Science, v. 247, p. 209–249.

—— 1964, Stable association wollastonite-anorthite, and other calc-silicate assemblages in amphibolite-facies crystalline schists of Nanga Parbat, northwest Himalayas: Beitrage zur Mineralogie und Petrographie, v. 10, p. 315–356.

Newton, R.C., and Haselton, H.T., 1981, Thermodynamics of the garnet-plagioclase-$Al_2SiO_5$-quartz geobarometer, *in* Newton, R.C., editor, Thermodynamics of Mineral and Melts: New York, Springer Verlag, p. 131–147.

Park, S. K., and Mackie, R.J., 1997, Crustal structure at Nanga Parbat, northern Pakistan, from magnetotelluric soundings: Geophysical Research Letters, v. 24, p. 2415–2418.

Pêcher, A., 1979, Les inclusions fluides des quartz d'exsudations de la zone du MCT Himalayan au Nepal central: donnees sur la phase fluid dans une grande zone de cisaillement crustal: Bulletin de Mineralogie, v. 102, p. 537–554.

Pognante, U., Benna, P., and Le Fort, P., 1993, High pressure metamorphism in the High-Himalayan Crystallines of the Stak Valley, northeastern Nanga Parbat-Haramosh Syntaxis, Pakistan, *in* Searle, M.P., and Treloar, P.J., editors, Himalayan Tectonics: Geological Society of London Special Publication 74, p. 161–172.

Pognante, U., and Spencer D.A., 1991, First report of eclogites from the Himalayan belt, Kaghan Valley (northern Pakistan): European Journal of Mineralogy, v. 3, p. 613–618.

Roedder, E., 1984, Fluid Inclusions: Mineralogical Society of America, Reviews in Mineralogy 12, Washington, D.C., 644 p.

Schneider, D.A., Edwards, M.A., Kidd, W.S.F., Asif Khan, M., Seeber, L., and Zeitler, P.K., 1999, Tectonics of Nanga Parbat, western Himalaya: Synkinematic plutonism within the doubly vergent shear zones of a crustal-scale pop-up structure: Geology, v. 27, p. 999–1002.

Smith, H.A., Chamberlain, C.P., and Zeitler, P.K., 1992, Documentation of Neogene regional metamorphism in the Himalayas of Pakistan using U-Pb in monazite: Earth and Planetary Science Letters, v. 113, p. 93–105.

——., 1994, Timing and duration of Himalayan metamorphism within the Indian Plate, northwest Himalaya, Pakistan: Journal of Geology, v. 102, p. 493–508.

Tahirkheli, R.A.K., Mattauer, M., Proust, F., and Tapponier, P., 1979, The India-Eurasia suture zone in northern Pakistan: some new data for an interpretation at plate scale, *in* Farah and Dejong, K.A., editors, Geodynamics of Pakistan: Quetta, Geological Survey of Pakistan, p. 130–135.

Tonarini, S., Villa, I., Oberli, F., Meier, M., Spencer, D.A., Pognante, U., and Ramsay, J.G., 1993, Eocene age of eclogite metamorphism in Pakistan Himalaya: implications for India-Eurasia collision: Terra Nova, v. 5, p. 13–20.

Treloar, P.J., Rex, D.C., Guise, P.G., Wheeler, J., and Hurford, A.J., 2000, Geochronological constraints on the evolution of the Nanga Parbat syntaxis, Pakistan Himalaya, *in* Khan, M.A., Treloar, P.J., Searle, M.P., and Jan, M.Q., editors, *in* Tectonics of the Nanga Parbat Syntaxis and the Western Himalaya: Geological Society of London Special Publication 170, p. 137–162.

Treloar, P.J., Rex, D.C., Guise, P.G., Coward, M.P., Searle, M.P., Windley, B.F., Petterson, M.G., Jan, M.Q., and Luff, I.W., 1989, K-Ar and Ar-Ar geochronology of the Himalayan collision in NW Pakistan: constraints on the timing of suturing, deformation, metamorphism and uplift: Tectonics, v. 8, p. 881–909.

Treloar, P.J., Rex, D.C., and Williams, M.P., 1991, The role of erosion and extension in unroofing the Indian Plate thrust stack, Pakistan Himalaya: Geological Magazine, v. 128, p. 465–478.

Treloar, P.J., Wheeler, J., and Potts, G.J., 1994, Metamorphism and melting within the Nanga Parbat syntaxis, Pakistan Himalaya: Mineralogical Magazine, v. 58A, p. 910–911.

Wheeler, J., Treloar, P.J., and Potts, G.J., 1995, Structural and metamorphic evolution of the Nanga Parbat syntaxis, Pakistan Himalayas, on the Indus gorge transect: the importance of early events: Geological Journal, v. 30, p. 349–371.

Whittington, A.G., 1996, Exhumation overrated at Nanga Parbat: Tectonophysics, v. 206, p. 215–226.

Whittington, A.G., Foster, G., Harris, N., Vance, D., and Ayres, M., 1999, Lithostratigraphic correlations in the western Himalaya–and isotopic approach: Geology, v. 27, p. 585–588.

Whittington, A.G., Harris, N., Baker, J., 1998, Low-pressure crustal anatexis: the significance of spinel and cordierite from metapelitic assemblages at Nanga Parbat, northern Pakistan, *in* Treloar, P.J. and O'Brien, P.J., editors, What Drives Metamorphism and Metamorphic Relations?: Geological Society Special Publications, v. 138, p. 183–198.

Whittington, A.G., Harris, N.B.W., Butler, R.W.H., 1999, Contrasting anatectic styles at Nanga Parbat, northern Pakistan, *in* Macfarlane, A., Sorkhabi, R.B., and Quade, J., editors, Himalaya and Tibet: Mountain Roots to Mountain Tops: Geological Society of America, Special Paper 138, p. 129–144.

Winslow, D. M., Chamberlain, C.P., and Zeitler, P.K., 1995, Metamorphism and melting of the lithosphere due to rapid denudation, Nanga Parbat Massif, Himalaya: Journal of Geology, v. 103, p. 395–409.

Winslow, D. M., Zeitler, P.K., Chamberlain, C.P., and Hollister, L.S., 1994, Direct evidence for a steep geotherm under conditions of rapid denudation, Western Himalaya, Pakistan: Geology, v. 22, p. 1075–1078.

Zeitler, P.K., 1985, Cooling history of the NW Himalaya, Pakistan: Tectonics, v. 4, p. 127–151.

Zeitler, P.K., and Chamberlain, C.P., 1991, Petrogenetic and tectonic significance of young leucogranites from the northwestern Himalaya, Pakistan: Tectonics, v. 10, p. 729–741.

Zeitler, P.K., Chamberlain, C.P., and Smith, H.A., 1993, Synchronous anatexis, metamorphism, and rapid denudation at Nanga Parbat (Pakistan Himalaya): Geology, v. 21, p. 347–350.

Zeitler, P.K., and Koons, P.O., 1998, Nanga Parbat as Tectonic Aneurysm: A metamorphic signature of indentor-corner dynamics: EOS (Transactions, American Geophysical Union), v. 79, p. F910.